This is a preprint, the final version is subject to change, of the American Mineralogist (MSA)
Cite as Authors (Year) Title. American Mineralogist, in press.
DOI: https://doi.org/10.2138/am-2019-6458

Revision 3 correction date 08.05.2019
Cation ordering, valence states and symmetry breaking in the crystal-chemically complex mineral chevkinite-(Ce). Recrystallization, transformation and metamict states in chevkinite

MARCIN STACHOWICZ[1,2,*], MARK D. WELCH[2], BOGUSŁAW BAGIŃSKI[1], PAVEL M. KARTASHOV[3], RAY MACDONALD[1], AND KRZYSZTOF WOŹNIAK[4]

[1]Institute of Geochemistry, Mineralogy and Petrology, University of Warsaw, 02-089 Warsaw, Poland.
[2]Department of Earth Sciences, The Natural History Museum, Cromwell Road, London SW7 5BD, England,
[3]Institute of Ore Deposits, Russian Academy of Sciences, Moscow 109107, Russia
[4]Biological and Chemical Research Centre, Chemistry Department, University of Warsaw, Żwirki i Wigury 101,02-089 Warszawa, Poland.

ABSTRACT

Annealing is commonly used in the recrystallization of metamict minerals in an attempt to reconstruct the original structure. Annealing at 750 °C of Nb-rich chevkinite-(Ce) from the Biraya rare-metal deposit, Russia, resulted in the structural transformation $C2/m \rightarrow P2_1/a$, which defines chevkinite crystal stability in different environments. This transformation seems to be a rapid version of a naturally occurring process that possibly involves twinning of the crystals. Nb-rich chevkinite-(Ce) occurs naturally as two polymorphs, one with the $C2/m$ space group and the other with $P2_1/a$. The latter is the stable form under ambient conditions. There are some distinct differences in the values of the structural parameters, such as the average *M*-O distances or site scattering values of particular sites for both space groups, which can be associated with the redistribution of some lighter cations, mainly Mg^{2+}, within the crystal lattice. The use of complementary experimental techniques (electron probe

microanalysis, X-ray diffraction, and photoelectron spectroscopy) has delivered information on the structure and transformation of a very complex, highly zoned and partially metamict solid solution. It should be useful in determining the structure of any mineral where cation disorder is present.

Keywords: chevkinite, annealing, crystal structure, metamict, recrystallization

INTRODUCTION

Chevkinite-group minerals (CGM), comprising twelve species, are increasingly being recognised as accessory phases in a wide range of igneous and metamorphic rocks (Macdonald and Belkin 2002; Vlach and Gualda 2007; Carlier and Lorand 2008; Belkin et al. 2009; Macdonald et al. 2009, 2012). The standard formula of CGM (Ito 1967), $A_4BC_2D_2(Si_2O_7)_2O_8$, is often used for determining the sites occupied by particular cations. Based on structural features CGM can be divided to two subgroups: chevkinite and perrierite. The chevkinite type structure is shown in summary form in Figure 1. Together CO_6 and DO_6 octahedra form sheets parallel to (001). Between these sheets are BO_6 octahedra, linked to neighbouring BO_6 and CO_6 octahedra by sharing corners with (Si_2O_7) disilicate groups, and *A* cations arranged in planar arrays with a Si(2)-centred tetrahedron inside each hexagonal array.

Due to the occurrence of CGM in chevkinite-type and perririte-type forms, there are also discrepancies in the assignment of ions to particular *B*, *C* and *D* sites. Previous studies of CGM have shown significant differences in the identification and names of unique sites of the crystal structure (particularly the *B*, *C* and *D* sites). To clarify which site in the crystal structure corresponds to a site from the empirical formula of Nb-rich chevkinite-(Ce)

determined by electron microprobe, a short graphical representation of the sites is presented in Figure 1. An alternative naming of *M*(1), *M*(2), *M*(3) and *M*(4), consistent with the nomenclature proposed by Hawthorne et al. (1995) and corresponding to *B*, *C*, *D*(1) and *D*(2), respectively, is given by Popov et al. (2001) and Sokolova et al. (2004). An exact definition of the sites in the crystal lattice is essential for a proper comparison with data available in the literature. An alternative description of the crystal structure of Fe-rich chevkinite-(Ce) was proposed by (Yang et al. 2002, 2007) with the unit cell origin shifted by the vector [0, 0, ½,]. Both descriptions are correct, but care must be taken when comparing the results in the literature. The coordinates (½,0, 0) correspond to the *B* site in Yang's et al. (2007) crystal structure and to the *D*(1) in our description and those of Popov et al. (2001) and Sokolova et al. (2004), who name it the *M*(3) site.

A concentration of radioactive elements often results in full or partial metamictization of the crystal structure (Hawthorne et al. 1991). This phenomenon has often been recognised for CGM (Sokolova et al. 2004), for which Th is a significant minor constituent. Annealing is often used to reconstruct a radiation-damaged crystal structure (Popov et al. 2001). Some areas of the studied samples of Nb-rich chevkinite-(Ce) are also metamict due to a significant concentration of Th (Stachowicz et al. 2019).

Thermal annealing can also cause the redistribution of metal cations between crystallographic sites. Rapid redistribution of cations on thermal annealing has been found in numerous minerals, such as amphibole (Reece et al. 2002; Welch et al. 2008, 2010; Zema et al. 2011) and olivine (Redfern et al. 1996) using X-ray and neutron diffraction. In these cases, progressive heating in 20 ºC steps from 200-800 ºC resulted in rapid redistribution of divalent cations (Mg^{2+}, Mn^{2+}, Fe^{2+}) within an hour. Consequently, it is likely that some cation redistribution will occur in chevkinite annealed at T >600 ºC for 24 hours.

Chevkinites are known to have vacancies at metal sites in the crystal structure, having been reported for the *A*, *B*, *C* and *D* sites (Yang et al. 2002), but at the *C* (*M*(*2*)) site only, varying from being minor (Popov et al. 2001; Sokolova et al. 2004) to the 50% vacancies at this site recorded in the crystal structure of delhuyarite-(Ce); this level of vacancy is species-defining (Holtstam et al. 2017).

There is also some uncertainty in the literature as to which space group(s) CGM belong to. $P2_1/a$ was determined by Čech et al. (1983), Haggerty and Mariano (1983), Miyawaki et al. (2002) and Xu et al. (2008). Space group $C2/m$ was proposed by Gottardi (1960), Yang et al. (1991), Popov et al. (2001), Yang et al. (2002, 2012) and Liziero (2008), whereas Miyajima et al. (2002) suggested that the structure of matsubaraite was in the pseudo-$C2/m$ group.

A sample of Nb-rich chevkinite-(Ce) from the Biraya rare-metal deposit, Russia, was studied by Stachowicz et al. (2019) to determine its crystal structure and to evaluate the role of Nb in the chevkinite group. Chevkinite from this locality is the most Nb-rich yet known. Stachowicz et al. (2019) identified a new substitution mechanism, $2\,{}^{D}Ti^{4+} \rightarrow {}^{D}Nb^{5+} + {}^{D}Ti^{3+}$, which, together with the substitution ${}^{C}Fe^{3+} + {}^{D}Ti^{4+} \rightarrow {}^{C}Fe^{2+} + {}^{D}Nb^{5+}$ leads to substantial Nb enrichment. The present paper focuses on the nature of the $P2_1/a$ phase in Nb-rich chevkinite-(Ce) from the same locality. On the basis of our new data, a possible relationship between the $P2_1/a$ and $C2/m$ space groups is proposed.

SAMPLE AND ANALYTICAL METHODS

The Nb-rich chevkinite-(Ce) analysed here is from the Biraya rare-metal deposit, located in the north of the Irkutsk district, Transbaikalia, Russia (57°52′51″N, 116°42′30″E). Nine single crystals were examined by single-crystal X-ray diffraction. Mineral compositions in crystal 1

were determined by electron microprobe at the Inter-Institute Analytical Complex at IGMiP Faculty of Geology, University of Warsaw, using a Cameca SX-100 microprobe equipped with four wavelength analysers. The detailed results are given in a companion article (Stachowicz et al., 2019). There is considerable compositional variation related to textural variations. Variation in the oscillatory zoned area is modest, e.g. 8.04-10.09 wt% Nb_2O_5. In that zone, the average analytical total is 98.03 wt%; however, a notable feature of the other zones is the low oxide totals, down to 88.41 wt%. Such low totals are commonly associated with hydrothermal alteration, consistent in this case with the textural evidence that the low-total zones appear to be replacing the oscillatory zones. The partial metamictization of the Nb-rich chevkinite-(Ce) crystals was confirmed by the results of series of X-ray experiments on natural and annealed crystals. The experimental section contains details of the annealing procedure. An analysis of the valences of Ce, Ti and Fe, investigated by X-ray photoelectron spectroscopy (XPS) was also presented (Stachowicz et al., 2019). Cerium is present as Ce^{3+} only, and iron as Fe^{2+} and Fe^{3+} in the ratio 1:1.84. Titanium is present in three valence states, +4, +3, +2, with ratios of 5:5:2, respectively. The EPMA analysis of unaltered parts of crystal 1 gave the following empirical formula:

$^{A}(Ca_{0.11}Na_{0.12}La_{1.30}Ce_{2.06}Pr_{0.16}Nd_{0.42})^{BCD}(Fe_{2.24}Mg_{0.22}Al_{0.15}Ti_{1.06}Nb_{0.98})(Si_{2.07}O_7)_2O_8$.

CRYSTAL STRUCTURE DETERMINATION

Experimental

A full Ewald sphere of reflections was collected to $\theta = 30^{\circ}$ for two crystals (1 and 6) using a KUMA KM4CCD κ-axis diffractometer equipped with Opal CCD detector and graphite-monochromated MoKα radiation. Another six crystals (2-5, 7, 8) from the same sample were analysed on an Agilent SuperNova diffractometer, equipped with a Mo Kα micro-focus X-ray

source and an EOS CCD detector. Finally, a series of single-crystal XRD experiments on crystal 9 was carried out with an Agilent XcaliburE diffractometer equipped with an EOS detector and MoKα radiation source.

Details of investigation of natural crystals 1 and 2 are given in the complementary paper (Stachowicz et al., 2019). Here, we present the results of the structural analysis of five additional natural crystals (3, 6, 7, 8, 9) and four annealed crystals (1, 4, 5, 9). The annealing of crystals 1, 4 and 5 was performed in a vacuum furnace at 750 °C, for 24 hours. The crystals were cooled to room temperature within three hours. A series of single-crystal XRD experiments on crystal 9 was carried out (i) on a natural, unheated crystal; (ii) after annealing at 500 °C for 24 h; (iii) after annealing at 600 °C for 18 h; (iv) after annealing at 600 °C for a further 24 h; (v) after annealing at 650 °C for 24 hours. Before each annealing cycle the crystal was enclosed in an evacuated borax glass capsule.

All data sets were corrected for Lorentz and polarization effects. A numerical absorption correction was applied in each case based upon crystal shape. Data reduction and analysis were carried out with the program CrysalisPro® (Rigaku-Oxford Diffraction).

Crystal structures were solved by direct methods and refined using SHELXL (Sheldrick 2008) as implemented in Olex2 (Dolomanov et al. 2009) and WinGX (Farrugia 2012). The refinements were based on F^2 for all reflections, except those with negative intensities. Weighted R factors (wR) and all goodness-of-fit (S) values are based on F^2. Conventional R factors are based on F with F set to zero for negative F^2. R factors based on F^2 are about twice as large as those based on F. Scattering factors for neutral atoms were taken from the International Tables for Crystallography Vol. C (Wilson 1992).

In order to obtain better geometry and ADPs (Sanjuan-Szklarz et al. 2016), higher-resolution datasets were collected than recommended by the International Union of Crystallography (IUCr). The highest residual electron density maxima (even up to 9.4 eÅ^{-3} for

crystal 2) are located *c.a.* 0.6-0.7 Å from the heavy *REE* atoms for all crystal structures. These values can be reduced (4.8 eÅ^{-3} for crystal 2) when the resolution is decreased to 0.6 Å^{-1}, (as recommended by IUCr), consistent with the cause of the high residual being associated with termination ripples in the Fourier synthesis, rather than being due to incomplete modelling of a contribution from non-bonded electrons or a split site.

In this study, the origin of the unit cell for all crystal structures was chosen such that the *B* site corresponds to the Wyckoff 2*d* unique position for space group *C*2/*m* and to the 2*b* position for space group $P2_1/a$. The unique site *C* refers to position 4*e* for both space groups. The *D* site refers to two independent Wyckoff positions: 2*a*, 2*b* for *C*2/*m* and 2*a*, 2*c* for $P2_1/a$. Our choice is analogous to that used by Sokolova et al. (2004).

Crystal structure data

Emphasis is given to the transformations of crystal 1 for which complementary X-ray datasets before and after annealing, and numerous electron probe microanalyzer (EPMA) analyses were obtained. Subsequent X-ray experiments on the remaining crystals (2-9) corroborate a general trend. The exact allocation of cations to crystallographic sites for compositions determined by EPMA is hindered for several reasons. The empirical formula for Nb-rich chevkinite-(Ce) crystal 1 given by Stachowicz et al. (2019) $^{A}(Ca_{0.18}Sr_{0.13}Na_{0.16}La_{1.2}Ce_{2.02}Pr_{0.16}Nd_{0.42})^{BCD}(Fe_{1.91}Mg_{0.16}Al_{0.13}Ti_{1.22}Nb_{1.11})(Si_{1.99}O_7)_2O_8$, is the average of all microprobe analyses, and is not representative because the crystal is partially metamict, due to its significant Th content. Partial recrystallization occurred during the annealing process, after which stronger scattering of X-rays by crystals 1 and 9 was observed. Moreover, the refined site scattering values (ssv= electrons per site) of the *A*, *B*, *C* and *D* sites changed. The transformation $C2/m \rightarrow P2_1/a$ was also observed. As described in the

Introduction, it is also likely that thermal annealing at 600-700 °C is involved in redistribution of some cations.

Initially, ssv were refined on the basis of the X-ray diffraction data. We found that an identical allocation of cations in both the $P2_1/a$ and $C2/m$ crystal structures is inconsistent with the refined site occupancies: *A*, *B*, *C* and *D* ssv sum to different values in the natural $C2/m$ and transformed, annealed $P2_1/a$ crystal 1. We carried out several X-ray experiments on both annealed and untreated natural crystals of Nb-rich chevkinite-(Ce) and found a clear correlation between the changes in the refined X-ray crystal structure parameters (Table 1) and the temperature of annealing.

The structural parameters for natural crystals 1, 6, 7, 8 and 9 listed in Table 1 are very consistent. Volumes of the first coordination spheres of cations at the *B*, *C* and *D* sites are similar for these ($C2/m$) crystals. BO_6 octahedra all have volumes of ~12 Å^3. *D*(1) and *D*(2) octahedra have equal volumes of ~11 Å^3. After annealing, the volume of the BO_6 octahedron increases markedly to 12.6 Å^3, whereas the volumes of CO_6, $D(1)O_6$ and $D(2)O_6$ octahedra remain unchanged. However, ssv values change for all *A*, *B*, *C* and *D*, being least for the *C* site. Crystals 2 and 3 are also natural, but their crystal structure parameters are comparable to those obtained for the annealed and transformed samples. The analysis of reflections (Figure S1) also proved that the space group for this case is rather $P2_1/a$.

DETERMINATION OF SPACE GROUPS

Consequences of crystal annealing; decrease of symmetry

In order to determine the space group(s) in which CGM crystallize the same single crystal fragment of Nb-rich chevkinite-(Ce) which was investigated using X-ray radiation (Stachowicz et al., 2019) was annealed at 750 °C for 24 hours, and then cooled to room

195 temperature within 3 hours. A new set of XRD data was then collected on our single crystal
196 X-ray diffractometer. Quasi-precession images of the (1*kl*) reciprocal lattice layer (Figure 2)
197 reconstructed from the full data collection prove the presence of the transformation from
198 *C*2/*m* space group to $P2_1/a$. Reflections violating *C*2/*m* symmetry ($h + k = 2n + 1$ for *hkl*) are
199 shown inside the red rectangles in Figure 2. The reconstructed diffraction patterns for the
200 fourteen X-ray experiments on Nb-rich chevkinite-(Ce) crystals are given in Supplementary
201 Figure S1, together with information on $<I/\sigma(I)>$ for all violators.
202 The natural crystals 2 and 3 also transformed to $P2_1/a$ symmetry and only these two
203 crystals exhibit a significant twinning out of all tested samples (1-9). It is, therefore, possible
204 that the mechanism of natural transformation involves twinning of the crystals.
205 Annealing of the Nb-rich chevkinite-(Ce) at 750°C caused a transition from space group
206 *C*2/*m* to $P2_1/a$ and we have suggested that this transformation seems to be a rapid version of a
207 naturally occurring process (Stachowicz et al. 2019). Evidence from the natural rocks is
208 equivocal. Perrierite, which generally forms at higher temperatures than chevkinite
209 (Macdonald and Belkin 2002; Macdonald et al. 2019), commonly but not invariably
210 crystallizes in space group $P2_1/a$; Sr-Zr perrierite-(Ce), for example, has a *C*2/*m* symmetry
211 (Stachowicz et al. 2014). Attempting to relate CGM space group type to temperature of
212 formation is hindered by the difficulties in estimating temperatures of the common host rocks,
213 such as metasomatites, skarns and pegmatites. Such information would be better sought using
214 phenocrysts in extrusive rocks for which temperatures have been estimated. A further
215 complication is that we have observed the reverse transformation from $P2_1/a$ to *C*2/*m* in a
216 compositionally simpler perrierite from Nettuno, Italy, induced by pressures up to 6 GPa.
217 The Bärnighausen tree (Figure 3) served as a test, validating the transition by means of
218 Group Theory. It summarises a transition pathway and was constructed using the
219 WYCKSPLIT (Kroumova et al. 1998) software implemented into the Bilbao Crystallographic

Server (Aroyo et al. 2006a, 2006b). The largest shift of atoms is expected for light atoms that are released from a symmetry element (O(3) and O(4)). The rotation of the SiO_4 tetrahedron, that contains O(3) and O(4) oxygen atoms, results in a change of the coordination of the *A*(2) site (see Table 1). A detailed discussion of the Bärnighausen tree and the symmetry relations in Nb-chevkinite-(Ce) is given in the Supplementary Data.

ASSIGNMENT OF POSITIONS FOR CATIONS

In order to determine which atoms occupy *A*, *B*, *C* and *D* sites, one can relate the values of the ionic radii (Shannon 1976) to the volumes of the first coordination polyhedra of each site, which can be calculated from the X-ray crystal structure using the algorithm introduced by Robinson et al. (1971). This approach may be useful especially in cases of a high variability of elements occupying the same crystallographic sites in a mineral, which is the case for Nb-rich chevkinite-(Ce). The volumes of octahedra were calculated in Platon software (Spek 2009) and the volumes of other polyhedra in Vesta software (Momma and Izumi 2011). The refined (against the X-ray data) *A*, *B*, *C* and *D* site scattering values sum to significantly different values for *C*2/*m* and $P2_1/a$ crystal structures. The MO_6 first coordination sphere octahedra (especially the BO_6 octahedra) also differ significantly in volume (Table 1).

The *A* sites are occupied by *REE*, Ca and Na atoms. As is common in CGM, there is an excess of elements in the *A* site. Sokolova et al. (2004) suggested the presence of small amounts of Ca (0.05 atoms per formula unit; apfu) in the *B* site of chevkinite-(Ce) from the Khaldzan Buragtag alkali granite, Mongolia.

The BO_6 octahedron is the largest of all MO_6 octahedra in CGM. The ions having the largest radii (except larger *REE* cations from the *A* sites) should be considered to occupy the *B* site. The ssv values of 26 electrons for natural (*C*2/*m*) crystals 1,7, 8 suggest the predominant occupancy of Fe^{2+} (ionic radius (i.r.) of 0.78 Å), which is in agreement with the literature. The

ssv values for crystals 6 and 9 suggest the possible occupation of elements heavier than Iron. Following the suggestion of Sokolova et al. (2004), due to the excess of cations commonly assigned to the *A* site, some can occupy also the *B* site of Nb-rich chevkinite-(Ce). Among heavier elements, only Th could fit in to this site: Th-O bond length varies between 2.15-2.62 Å for crystal structures with Th-O_6 coordination octahedra (Serezhkina et al. 2017). Figure 4 presents the BO_6 coordination with atoms shown as thermal ellipsoids. Mixed occupancy can be registered as a larger U_{iso} value and prolate/oblate anisotropic displacement ellipsoid. However, a positional disorder of a single atom species must also be considered. To reach the ssv of 29 for crystal 9, 0.08 *apfu* of Th^{4+} in the *B* site is needed and 0.04 *apfu* to reach an ssv of 27.6 for crystal 6. Crystal 9 was also much more metamict than other crystals (see Supplementary Figure S1 with the weakest scattering of X-ray reflections, despite the longest exposure time), so a larger concentration of Th is expected here. The mechanism of Th incorporation into the *B* site may be the substitution: ${}^{B}Fe^{2+} + {}^{A}Ce^{3+} \rightarrow {}^{B}Th^{4+} + {}^{A}Na^{+}$.

With the transformation to a lower symmetry space group the volume of BO_6 increases on the average by 0.6 $Å^3$ and the ssv value drops by *ca.* 2 electrons. These results show that heating induces a reorganisation or substitution of cations. The lighter Mg^{2+} (i.r. =0.72Å) ions substitute for Th^{4+} or part of the Fe^{2+}.

The *C* site has the smallest volume of all MO_6 coordination octahedra (Table 1) for Nb-rich chevkinite-(Ce) (for both structure types). It is occupied by Fe^{3+} (i.r.= 0.65 Å), Nb^{5+} (i.r.= 0.64 Å) and Al^{3+} (i.r.= 0.54 Å) ions. This site shows the smallest changes due to transformation, both in CO_6 volume and ssv values.

The two *D*(1) and *D*(2) sites have identical DO_6 volumes, yet differ with ssv values of 20.7 and 24.2 in average, respectively, for crystals of *C*2/*m* symmetry. We assigned Ti^{3+} (i.r.= 0.67 Å), Ti^{4+} (i.r.= 0.60 Å), Nb^{5+} and Mg^{2+}into these sites. In the transformed crystals ($P2_1/a$ symmetry), Mg^{2+} is absent from these sites which is reflected in the increase of ssv to 24.7

and 26.8 in average, for *D*(1) and *D*(2) respectively. The DO_6 octahedra have the largest volumes (our calculations) among all chevkinites of known crystal structure. We interpret this as a structural indication of the presence of Ti^{3+} (*C*2/*m* and $P2_1/a$) and Mg^{2+} (*C*2/*m*) at the *D* sites of the Nb-rich chevkinite-(Ce). The mechanism of Ti^{4+} substitution in the D sites is also proposed as: $2Ti^{4+} \rightarrow Nb^{5+} + Ti^{3+}$; $2Ti^{4+} + O^{2-} \rightarrow Nb^{5+} + Mg^{2+} + OH^{-}$ + vac.

Niobium is distributed among the *C* and *D* sites. Its presence is shown in larger values of ssv because it is masked by the presence of vacancies and lighter elements, Al^{3+} at the *C* and Mg^{2+} at the *D* site. With the migration of Magnesium to the *B* site in the $P2_1/a$ crystal structure the presence of Nb is revealed in the increasing values of ssv of the *D* sites.

IMPLICATIONS

The recognition that the analysis of the systematic extinction of reflections forbidden in a certain space group can be equivocal demands testing. Such a test, proposed here, is the values of the volumes of BO_6 octahedra and atomic displacement parameters U_{eq}. A convenient tool in the evaluation of indicators of the crystal symmetry is construction of the Bärnighausen tree. The multidisciplinary crystal-chemical approach used here should be of value in determining the structure of all minerals with cation disorder. This may be particularly relevant to REE-bearing phases due to the increased use of REE in technological applications and the accompanying interest in REE exploitation.

The possible existence of a new end member in CGM has been identified with the substitution mechanism given for Ti^{3+} and Nb^{5+} in the D sites: ${}^{A}Ce_4{}^{B}Fe^{2+}{}^{C}(Fe^{3+})_2{}^{D}Nb^{5+}{}^{D}Ti^{3+}(Si_2O_7)_2O_8$.

Geological significance

Nb-rich chevkinite-(Ce) is of igneous/hydrothermal origin. We can speculate that the mineral was formed at relatively high temperature and then rapidly cooled. The cooling froze the structure in space group *C*2/*m* which is stable at high temperature but remains metastable

295 at room temperature. It can be assumed that the metastable phase at room temperature would,
296 after a sufficiently long time, reorganise to a lower symmetry. Laboratory heating of the
297 sample delivered enough energy to overcome the kinetic barrier of the transition and enabled
298 the ordering of most of the atoms in the general positions of the unit cell. The energy supplied
299 to the system was not large enough to match the natural conditions for the formation of Nb-
300 rich chevkinite-(Ce) and that is why we were able to recognise the crystal structure
301 transformation.
302

303 ## ACKNOWLEDGMENTS

304 We are very grateful to David Brown, an anonymous reviewer and Associate Editor
305 Alejandro Fernandez-Martinez for their very helpful comments on the manuscript, which
306 much improved its quality. The research for this paper was in part supported by the Polish
307 Ministry of Science and Higher Education within the Mobility Plus Fund award number
308 1301/MOB/IV/2015/0. Financial support was provided by Polish National Science Centre
309 NCN grant decision DEC-2011/03/B/ST10/05491. We thank the Department of Earth
310 Sciences, Natural History Museum, London, for hosting MS's year-long visit to work with
311 MDW.
312

313 ## REFERENCES CITED

314 Aroyo, M.I., Perez-Mato, J.M., Capillas, C., Kroumova, E., Ivantchev, S., Madariaga, G.,
315 Kirov, A., and Wondratschek, H. (2006a) Bilbao Crystallographic Server: I. Databases
316 and crystallographic computing programs. Zeitschrift für Kristallographie, 221, 15–27.
317 Aroyo, M.I., Kirov, A., Capillas, C., Perez-Mato, J.M., and Wondratschek, H. (2006b) Bilbao
318 Crystallographic Server. II. Representations of crystallographic point groups and space

groups. Acta Crystallographica Section A Foundations of Crystallography, 62, 115–128.

Bader, R.F.W. (1994) Atoms in Molecules: A Quantum Theory, 438 p. Clarendon Press.

Bader, R.F.W. (1998) A Bond Path: A Universal Indicator of Bonded Interactions. The Journal of Physical Chemistry A, 102, 7314–7323.

Belkin, H.E., Macdonald, R., and Grew, E.S. (2009) Chevkinite-group minerals from granulite-facies metamorphic rocks and associated pegmatites of East Antarctica and South India. Mineralogical Magazine, 73, 149–164.

Carlier, G., and Lorand, J.-P. (2008) Zr-rich accessory minerals (titanite, perrierite, zirconolite, baddeleyite) record strong oxidation associated with magma mixing in the south Peruvian potassic province. Lithos, 104, 54–70.

Čech, F., Povondra, P., and Vrâna, S. (1983) Crystal chemistry of a chevkinite from Zambia. Acta Universitatis Carolinae – Geologica, 181–193.

Dolomanov, O.V., Bourhis, L.J., Gildea, R.J., Howard, J.A.K., and Puschmann, H. (2009) *OLEX2* : a complete structure solution, refinement and analysis program. Journal of Applied Crystallography, 42, 339–341.

Farrugia, L.J. (2012) WinGX and ORTEP for Windows: an update. Journal of Applied Crystallography, 45.

Gottardi, Y. (1960) The crystal structure of perrierite. The American Mineralogist, 45, 1–14.

Haggerty, S.E., and Mariano, A.N. (1983) Strontian-loparite and strontio-chevkinite: Two new minerals in rheomorphic fenites from the Paraná Basin carbonatites, South America. Contributions to Mineralogy and Petrology, 84, 365–381.

Hawthorne, F.C., Groat, L.A., Raudsepp, M., Ball, N.A., Kimata, M., Spike, F.D., Gaba, R., Halden, N.M., Lumpkin, G.R., and Ewing, R.C. (1991) Alpha-decay damage in titanite. American Mineralogist, 76, 370–396.

Hawthorne, F.C., Ungaretti, L., and Oberti, R. (1995) Site populations in minerals; terminology and presentation of results of crystal-structure refinement. The Canadian Mineralogist, 33, 907–911.

Holtstam, D., Bindi, L., Hålenius, U., and Andersson, U.B. (2017) Delhuyarite-(Ce) – $Ce_4Mg(Fe^{3+}_2W)□(Si_2O_7)_2O_6(OH)_2$ – a new mineral of the chevkinite group, from the Nya Bastnäs Fe–Cu–REE deposit, Sweden. European Journal of Mineralogy, 29, 897–905.

Ito, J. (1967) A Study of Chevkinite and Perrierite. The American Mineralogist, 52, 1094–1104.

Kroumova, E., Perez-Mato, J.M., and Aroyo, M.I. (1998) WYCKSPLIT: a computer program for determination of the relations of Wyckoff positions for a group-subgroup pair. Journal of Applied Crystallography, 31, 646–646.

Liziero, F. (2008) Studio Cristallochimico E Strutturale Di Chevkiniti-(Ce) Non Metamittiche. Ph.D. thesis.

Macdonald, R., and Belkin, H.E. (2002) Compositional variation in minerals of the chevkinite group. Mineralogical Magazine, 66, 1075–1098.

Macdonald, R., Belkin, H.E., Wall, F., and Bagiński, B. (2009) Compositional variation in the chevkinite group: new data from igneous and metamorphic rocks. Mineralogical Magazine, 73, 777–796.

Macdonald, R., Bagiński, B., Kartashov, P., Zozulya, D., and Dzierżanowski, P. (2012) Chevkinite-group minerals from Russia and Mongolia: new compositional data from metasomatites and ore deposits. Mineralogical Magazine, 76, 535–549.

Macdonald, R., Bagiński, B., Belkin, H.E., and Stachowicz, M. (2019) Composition, paragenesis, and alteration of the chevkinite group of minerals. American Mineralogist, 104, 348–369.

Miyajima, H., Miyawaki, R., Ito, K., Miyajima, H., Miyawaki, R., and Ito, K. (2002) Matsubaraite, $Sr_4Ti_5(Si_2O_7)_2O_8$, a new mineral, the Sr-Ti analogue of perrierite in jadeitite from the Itoigawa-Ohmi district, Niigata Prefecture, Japan. European Journal of Mineralogy, 14, 1119–1128.

Miyawaki, R., Matsubara, S., and Miyajima, H. (2002) The crystal structure of rengeite, $Sr_4ZrTi_4(Si_2O_7)_2O_8$. Journal of Mineralogical and Petrological Sciences, 97, 7–12.

Momma, K., and Izumi, F. (2011) *VESTA 3* for three-dimensional visualization of crystal, volumetric and morphology data. Journal of Applied Crystallography, 44, 1272–1276.

Nespolo, M. (2008) Does mathematical crystallography still have a role in the XXI century? Acta Crystallographica Section A Foundations of Crystallography, 64, 96–111.

Popov, V.A., Pautov, L.A., Sokolova, E., Hawthorne, F.C., McCammon, C., and Bazhenova, L.F. (2001) Polyakovite-(Ce),(REE, Ca)$_4$(Mg, Fe^{2+})(Cr^{3+}, Fe^{3+})$_2$(Ti, Nb)$_2Si_4O_{22}$, a new metamict mineral species from the Ilmen Mountains, southern Urals, Russia: mineral description and crystal chemistry. The Canadian Mineralogist, 39, 1095–1104.

Redfern, S.A.T., Henderson, C.M.B., Wood, B.J., Harrison, R.J., and Knight, K.S. (1996) Determination of olivine cooling rates from metal-cation ordering. Nature, 381, 407.

Reece, J.J., Redfern, S.A.T., Welch, M.D., Henderson, C.M.B., and McCammon, C.A. (2002) Temperature-dependent Fe 2+ -Mn 2+ order-disorder behaviour in amphiboles. Physics and Chemistry of Minerals, 29, 562–570.

Robinson, K., Gibbs, G.V., and Ribbe, P.H. (1971) Quadratic Elongation: A Quantitative Measure of Distortion in Coordination Polyhedra. Science, 172, 567–570.

Sanjuan-Szklarz, W.F., Hoser, A.A., Gutmann, M., Madsen, A.Ø., and Woźniak, K. (2016) Yes, one can obtain better quality structures from routine X-ray data collection. IUCrJ, 3, 61–70.

Serezhkina, L.B., Savchenkov, A.V., and Serezhkin, V.N. (2017) Stereochemistry of thorium in oxygen-containing compounds. Russian Journal of Inorganic Chemistry, 62, 633–638.

Shannon, R.D. (1976) Revised effective ionic radii and systematic studies of interatomic distances in halides and chalcogenides. Acta Crystallographica Section A, 32, 751–767.

Sheldrick, G.M. (2008) A short history of *SHELX*. Acta Crystallographica Section A Foundations of Crystallography, 64, 112–122.

Sokolova, E., Hawthorne, F.C., Ventura, G.D., and Kartashov, P.M. (2004) Chevkinite-(Ce): Crystal Structure and the Effect of Moderate Radiation-Induced Damage on Site-Occupancy Refinement. The Canadian Mineralogist, 42, 1013–1025.

Spek, A.L. (2009) Structure validation in chemical crystallography. Acta Crystallographica Section D Biological Crystallography, 65, 148–155.

Stachowicz, M., Bagiński, B., Macdonald, R., Kartashov, P.M., Oziębło, A., and Woźniak, K. (2014) Structure of Sr-Zr-bearing perrierite-(Ce) from the Burpala Massif, Russia. Mineralogical Magazine, 78, 1647–1659.

Stachowicz, M., Bagiński, B., Welch, M.D., Kartashov, P.M., Macdonald, R., Balcerzak, J., Tyczkowski, J., and Woźniak, K. (2019) Cation ordering, valence states, and symmetry breaking in the crystal-chemically complex mineral chevkinite-(Ce): X-ray diffraction and photoelectron spectroscopy studies and mechanisms of Nb enrichment. American Mineralogist, 104, 595–602.

Vlach, S.R.F., and Gualda, G.A.R. (2007) Allanite and chevkinite in A-type granites and syenites of the Graciosa Province, southern Brazil. Lithos, 97, 98–121.

Welch, M.D., Reece, J.J., and Redfern, S.A.T. (2008) Rapid intracrystalline exchange of octahedrally-coordinated divalent cations in amphiboles: an in situ high-temperature

neutron diffraction study of synthetic potassic richterite $^{A}K^{B}(NaCa)^{C}(Mg_{2.5}Ni_{2.5})Si_8O_{22}(OH)_2$. Mineralogical Magazine, 72, 877–886.

Welch, M.D., Cámara, F., and Oberti, R. (2010) Thermoelasticity and high-T behaviour of anthophyllite. Physics and Chemistry of Minerals, 38, 321–334.

Wilson, A.J.C. (1992) International Tables for Crystallography: Mathematical, physical, and chemical tables Vol. 3. International Union of Crystallography.

Xu, J., Yang, G., Li, G., Wu, Z., and Shen, G. (2008) Dingdaohengite-(Ce) from the Bayan Obo REE-Nb-Fe Mine, China: Both a true polymorph of perrierite-(Ce) and a titanic analog at the C1 site of chevkinite subgroup. American Mineralogist, 93, 740–744.

Yang, G. (1991) New investigation on the space group of chevkinite. Journal of China University of Geosciences, 2, 75–78.

Yang, Z., Fleck, M., Smith, M., Tao, K., Song, R., and Zhang, P. (2002) The crystal structure of natural Fe-rich chevkinite-(Ce). European Journal of Mineralogy, 14, 969–975.

Yang, Z., Li, H., Liu, M., and Franz, P. (2007) Crystal Chemistry of Iron in Non-Metamict Chevkinite-(Ce): Valence State and Site Occupation Proportions. Journal of Rare Earths, 25, 238–242.

Yang, Z., Giester, G., Ding, K., and Tillmanns, E. (2012) Hezuolinite, $(Sr,REE)_4Zr(Ti,Fe^{3+},Fe^{2+})_2Ti_2O_8(Si_2O_7)_2$, a new mineral species of the chevkinite group from Saima alkaline complex, Liaoning Province, NE China. European Journal of Mineralogy, 24, 189–196.

Zema, M., Welch, M.D., and Oberti, R. (2011) High-T behaviour of gedrite: thermoelasticity, cation ordering and dehydrogenation. Contributions to Mineralogy and Petrology, 163, 923–937.

FIGURE CAPTIONS

Figure 1. Unit cell oriented along the **b** direction. The positions of the MO_6 coordination octahedra of *B*, *C* and *D* sites are in green, yellow and orange, respectively. *M*(1)-*M*(4) is an alternative naming of sites first proposed by Popov et al. (2001).

Figure 2. Comparison of precession images of (1kl) layers for (a) untreated crystal 1 in *C*2/*m* symmetry and (b) in $P2_1/a$ symmetry, after annealing at 750 °C. The reflection extinction rule for *C* centring of the unit cell, h+k = 2n+1 for all (hkl) reflections, does not hold for the annealed crystal (b).

Figure 3. The Bärnighausen tree indicates a transition from aristoptype *C*2/*m* to a hettotype $P2_1/a$. Above the arrows are given the shifts of atoms in Å. Below the diagram are given the three oxygen atoms that with the transformation symmetry in aristotype correspond to the O(1A), O(5A) and O(8A) atoms from the hettotype.

Figure 4. The *B*-O bonds in BO_6 coordination. The broken-off bond of 2.16 Å corresponds to the extremal position of an O(3) atom.

This is a preprint, the final version is subject to change, of the American Mineralogist (MSA)
Cite as Authors (Year) Title. American Mineralogist, in press.
DOI: https://doi.org/10.2138/am-2019-6458

TABLES

Table 1. The M-O bond distances and site scattering values (ssv) for *A*,*B*,*C* and *D* sites in Nb-rich chevkinite-(Ce), for crystals 1-9 – distances in Å, together with volumes (V in Å^3) of the MO_x first coordination spheres. Crystal numbers are given in the second row with temperature of annealing as superscript.

*C*2/*m*	1	6	7	8	9	*P*2$_1$/*a*	9$_{an}^{600}$	9$_{an2}^{600}$	9$_{an3}^{650}$	2	3	4$_{an}^{750}$	5$_{an}^{750}$	1$_{an}^{750}$
***A*(1)**						***A*(1)**								
O(8) $_{x2}$	2.491(5)	2.487(4)	2.495(3)	2.495(4)	2.489(5)	**O(8A)**	2.471(4)	2.467(4)	2.465(3)	2.472(6)	2.472(7)	2.441(2)	2.441(2)	2.463(3)
						O(8)	2.490(4)	2.490(4)	2.500(3)	2.512(6)	2.524(7)	2.513(2)	2.515(2)	2.517(3)
O(2)	2.496(6)	2.496(6)	2.499(5)	2.500(6)	2.517(9)	**O(2)**	2.496(4)	2.493(4)	2.489(3)	2.505(7)	2.503(8)	2.469(2)	2.481(2)	2.482(3)
						O(1A)	2.500(4)	2.499(4)	2.483(4)	2.481(7)	2.471(7)	2.427(2)	2.454(2)	2.462(4)
O(1) $_{x2}$	2.542(7)	2.553(5)	2.549(5)	2.544(6)	2.551(7)	**O(1)**	2.545(4)	2.546(4)	2.557(4)	2.553(7)	2.565(7)	2.564(2)	2.590(2)	2.563(4)
O(5) $_{x2}$	2.560(6)	2.559(4)	2.560(4)	2.558(4)	2.560(5)	**O(5)**	2.573(4)	2.575(4)	2.578(3)	2.572(6)	2.575(6)	2.566(2)	2.574(2)	2.581(3)
						O(5A)	2.574(4)	2.572(4)	2.580(4)	2.574(6)	2.574(7)	2.575(2)	2.585(2)	2.582(3)
O(7)	2.810(6)	2.806(4)	2.813(4)	2.811(4)	2.800(7)	**O(7)**	2.817(3)	2.819(3)	2.828(3)	2.826(7)	2.834(7)	2.854(2)	2.839(2)	2.846(3)
<M-O>	2.56(2)	2.56(2)	2.57(2)	2.56(2)	2.56(2)	**<M-O>**	2.56(2)	2.56(2)	2.56(1)	2.56(2)	2.56(2)	2.55(2)	2.56(6)	2.56(1)
V *AO*$_8$	28.1	28.1	28.2	28.1	28.3	**V *AO*$_8$**	28.3	28.0	28.0	28.1	28.2	27.6	27.9	28.0
O(4) $_{x2}$	3.189(3)	3.189(4)	3.197(3)	3.196(4)	3.199(5)	**O(4)**	3.144(6)	3.131(5)	3.092(5)	3.057(7)	3.018(8)	2.948(2)	2.919(3)	3.011(4)
						<M-O>	2.62(2)	2.62(2)	2.62(1)	2.62(2)	2.62(2)	2.595(5)	2.600(6)	2.61(1)
						V *AO*$_9$	32.7	32.6	32.6	32.6	32.6	31.8	32.2	32.4
						O(3)*	3.315(4)	3.313(4)	3.310(3)	3.32(1)	3.318(7)	3.251(2)	3.301(3)	3.319(3)
<M-O>	2.69(2)	2.69(2)	2.69(2)	2.69(2)	2.69(2)	**<M-O>**	2.69(2)	2.69(2)	2.69(2)	2.69(2)	2.69(2)	2.66(2)	2.67(8)	2.68(2)
V *AO*$_{10}$	37.8	37.8	37.9	37.8	38.0	**V *AO*$_{10}$**	38.0	38.4	38.4	38.4	38.4	37.5	37.9	38.3
ssv	52.5	52.7	51.9	52.1	52.2	**ssv**	54.7	55.2	55.8	52.2	53.7	52.7	55.7	55.2
***A*(2)**						***A*(2)**								
O(2)	2.454(7)	2.456(6)	2.450(5)	2.445(6)	2.469(9)	**O(2)**	2.438(4)	2.435(4)	2.434(3)	2.420(7)	2.423(8)	2.407(2)	2.435(2)	2.431(3)
O(8) $_{x2}$	2.499(5)	2.493(4)	2.499(3)	2.502(4)	2.492(5)	**O(8)**	2.485(4)	2.485(4)	2.477(3)	2.484(6)	2.482(7)	2.457(2)	2.454(2)	2.475(3)
						O(8A)	2.526(4)	2.529(4)	2.545(3)	2.557(6)	2.565(7)	2.576(2)	2.571(2)	2.571(3)
O(1) $_{x2}$	2.703(7)	2.693(5)	2.682(5)	2.683(6)	2.698(7)	**O(1)**	2.626(4)	2.624(4)	2.612(4)	2.615(7)	2.599(7)	2.549(2)	2.576(2)	2.589(4)
O(6)	2.632(6)	2.627(4)	2.637(4)	2.631(5)	2.634(7)	**O(1A)**	2.662(4)	2.658(4)	2.661(4)	2.663(7)	2.669(7)	2.673(2)	2.696(2)	2.663(4)

O(5) $_{x2}$	2.605(5)	2.601(4)	2.605(4)	2.606(4)	2.611(5)	**O(5A)**	2.619(4)	2.615(4)	2.623(4)	2.628(6)	2.629(7)	2.613(2)	2.603(2)	2.636(3)
						O(5)	2.615(4)	2.610(4)	2.616(3)	2.613(6)	2.617(6)	2.620(2)	2.613(2)	2.625(3)
						O(6)	2.627(3)	2.624(3)	2.630(3)	2.624(7)	2.631(8)	2.624(2)	2.627(2)	2.637(3)
<M-O>	2.59(2)	2.58(2)	2.58(2)	2.58(2)	2.59(2)	**<M-O>**	2.57(2)	2.57(2)	2.57(1)	2.58(3)	2.58(3)	2.56(3)	2.57(6)	2.58(1)
V *AO*$_8$	28.2	28.5	28.5	28.5	28.8	**V *AO*$_8$**	28.1	28.1	28.1	28.2	28.2	27.7	27.9	28.2
O(3) $_{x2}$	3.034(3)	3.030(2)	3.028(2)	3.027(2)	3.032(3)	**O(3)**	2.890(6)	2.871(5)	2.816(5)	2.803(7)	2.745(7)	2.644(2)	2.652(2)	2.716(4)
						<M-O>	2.61(3)	2.61(2)	2.60(2)	2.60(2)	2.60(2)	2.574(5)	2.580(6)	2.60(1)
						V *AO*$_9$	33.0	32.8	32.8	32.9	32.8	32.1	32.4	32.7
						O(3)*	3.117(6)	3.135(5)	3.185(5)	3.211(9)	3.263(7)	3.308(2)	3.336(2)	3.275(4)
<M-O>	2.68(2)	2.67(2)	2.67(2)	2.67(2)	2.68(2)	**<M-O>**	2.66(2)	2.66(2)	2.66(2)	2.66(3)	2.66(3)	2.65(3)	2.66(7)	2.66(1)
V *AO*$_{10}$	38.8	38.6	38.6	38.6	38.8	**V *AO*$_{10}$**	38.2	38.1	38.2	38.3	38.3	37.5	37.9	38.2
ssv	50.2	51.0	50.2	50.4	51.3	**ssv**	53.5	53.9	54.8	51.6	52.9	50.8	55.2	54.1
B						***B***								
O(3) $_{x2}$	1.988(8)	1.982(7)	1.989(6)	1.988(7)	2.004(11)	**O(3)**$_{x2}$	2.015(4)	2.012(3)	2.019(3)	2.010(8)	2.006(8)	2.016(2)	2.010(2)	2.026(3)
O(1) $_{x4}$	2.156(6)	2.151(6)	2.165(5)	2.167(6)	2.164(7)	**O(1)**$_{x2}$	2.214(4)	2.212(4)	2.213(4)	2.212(7)	2.213(7)	2.194(2)	2.184(2)	2.217(4)
						O(1A)$_{x2}$	2.223(4)	2.216(4)	2.228(4)	2.233(7)	2.229(7)	2.219(2)	2.211(2)	2.238(4)
<M-O>	2.10(2)	2.10(2)	2.11(2)	2.11(2)	2.11(3)	**<M-O>**	2.15(1)	2.15(1)	2.15(1)	2.15(2)	2.15(2)	2.143(5)	2.135(5)	2.16(1)
V *BO*$_6$	12.0	11.9	12.0	12.0	12.1	**V *BO*$_6$**	12.6	12.6	12.7	12.6	12.6	12.4	12.4	12.8
ssv	25.9	27.6	26.0	26.2	29.0	**ssv**	25.2	25.2	25.1	24.6	24.4	25.5	23.5	25.0
C						***C***								
O(7) $_{x2}$	1.969(4)	1.968(3)	1.971(3)	1.972(4)	1.976(5)	**O(7)**$^{\#}$	1.974(4)	1.975(3)	1.976(3)	1.981(7)	1.972(6)	1.941(2)	1.949(2)	1.977(3)
O(6) $_{x2}$	1.978(4)	1.979(4)	1.980(3)	1.979(4)	1.989(5)	**O(6)**$^{\$}$	1.987(4)	1.986(3)	1.987(3)	1.977(6)	1.983(6)	1.961(2)	1.962(2)	1.988(3)
						O(7)*	1.980(4)	1.981(3)	1.983(3)	1.979(7)	1.980(6)	1.964(2)	1.975(2)	1.985(3)
						O(6)*	1.993(4)	1.995(3)	2.000(3)	1.994(6)	2.003(6)	1.985(2)	1.993(2)	2.005(3)
O(5) $_{x2}$	2.017(4)	2.019(3)	2.019(3)	2.019(3)	2.036(4)	**O(5)**	2.031(4)	2.034(3)	2.034(3)	2.020(6)	2.028(6)	2.015(2)	2.028(2)	2.032(3)
						O(5A)	2.026(3)	2.029(3)	2.029(3)	2.020(6)	2.032(6)	2.009(2)	2.022(2)	2.029(3)
<M-O>	1.99(1)	1.999(9)	1.990(7)	1.990(9)	2.00(2)	**<M-O>**	2.00(1)	2.000(8)	2.002(8)	1.99(2)	2.00(2)	1.979(5)	1.988(5)	2.003(8)

V *C*O$_6$	10.4	10.4	10.4	10.4	10.6	**V *C*O$_6$**	10.6	10.6	10.6	10.5	10.6	10.3	10.4	10.6
ssv	24.4	24.2	24.2	24.4	24.1	**ssv**	23.8	24.0	24.1	22.7	23.2	21.4	22.6	23.7
***D*(1)**						***D*(1)**								
O(8) $_{x4}$	2.013(4)	2.015(4)	2.008(3)	2.006(4)	2.028(5)	**O(8) $_{x2}$**	2.020(4)	2.020(3)	2.023(3)	2.017(6)	2.009(7)	1.986(2)	2.003(2)	2.022(3)
						O(8A) $_{x2}$	2.004(4)	2.005(3)	2.005(3)	1.995(6)	1.984(7)	1.964(2)	1.978(2)	2.002(3)
O(6) $_{x2}$	2.043(5)	2.040(5)	2.038(4)	2.039(5)	2.039(7)	**O(6) $_{x2}$**	2.027(3)	2.026(3)	2.026(3)	2.038(7)	2.021(7)	2.017(2)	2.028(2)	2.024(3)
<M-O>	2.02(2)	2.02(2)	2.018(9)	2.02(1)	2.03(2)	**<M-O>**	2.02(1)	2.017(8)	2.018(8)	2.02(2)	2.02(2)	1.989(5)	2.003(5)	2.016(8)
V *D*O$_6$	11.0	11.0	10.9	10.9	11.1	**V *D*O$_6$**	10.9	10.9	10.9	10.9	10.7	10.4	10.7	10.9
ssv	20.8	20.6	20.9	21.2	20.0	**ssv**	25.6	26.5	27.4	22.7	23.1	23.8	24.6	23.7
***D*(2)**						***D*(2)**								
O(7) $_{x2}$	2.039(5)	2.035(4)	2.032(4)	2.029(5)	2.041(7)	**O(7) $_{x2}$**	2.021(3)	2.018(3)	2.019(3)	2.020(6)	2.019(7)	1.984(2)	2.022(2)	2.017(3)
O(8) $_{x4}$	2.011(4)	2.013(4)	2.012(3)	2.008(4)	2.021(5)	**O(8) $_{x2}$**	2.017(4)	2.016(3)	2.019(3)	1.999(6)	1.985(7)	2.012(2)	1.991(2)	2.016(3)
						O(8A) $_{x2}$	2.030(4)	2.033(3)	2.036(3)	2.023(6)	2.026(7)	2.016(2)	2.029(2)	2.044(3)
<M-O>	2.02(2)	2.02(1)	2.019(9)	2.02(2)	2.03(2)	**<M-O>**	2.02(1)	2.022(8)	2.025(8)	2.01(2)	2.01(2)	2.003(5)	2.014(5)	2.026(8)
V *D*O$_6$	11.0	11.0	10.9	10.9	11.1	**V *D*O$_6$**	11.0	11.0	11.0	10.8	10.8	10.7	10.8	11.0
ssv	24.5	24.3	24.1	24.3	23.7	**ssv**	27.0	27.9	28.5	26.0	25.6	24.4	24.9	30.4

[#]x,y,z; [$]x,y,1+z; [*]3/2-x,-1/2+y,1-z

This is a preprint, the final version is subject to change, of the American Mineralogist (MSA)
Cite as Authors (Year) Title. American Mineralogist, in press.
DOI: https://doi.org/10.2138/am-2019-6458

463 **FIGURES**

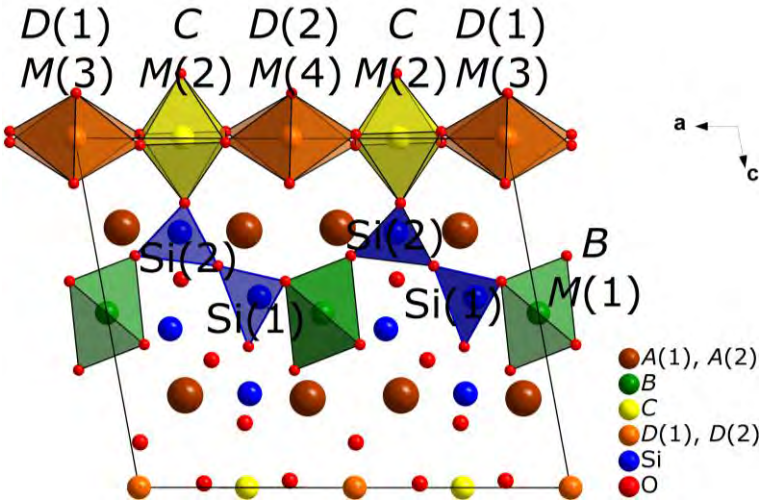

464

465 **Figure 1**. Unit cell oriented along the b direction. The positions of the MO_6 coordination octahedra of *B*, *C*
466 and *D* sites are in green, yellow and orange, respectively. *M*(1)-*M*(4) is an alternative naming of sites first
467 proposed by Popov et al. (2001).

468

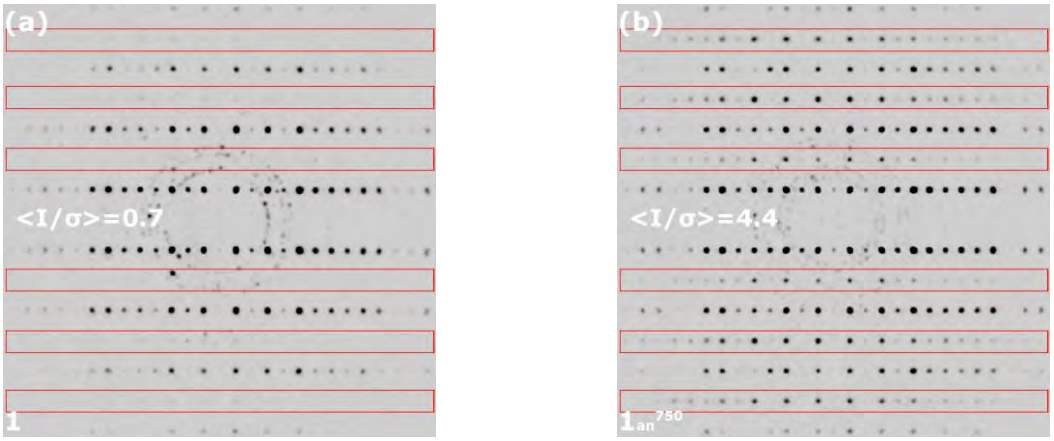

469 **Figure 2.** Comparison of precession images of (1kl) layers for (a) untreated crystal 1 in *C*2/*m* symmetry and
470 (b) in $P2_1/a$ symmetry, after annealing at 750 °C. The reflection extinction rule for *C* centring of the unit
471 cell, h+k = 2n+1 for all (hkl) reflections, does not hold for the annealed crystal (b).

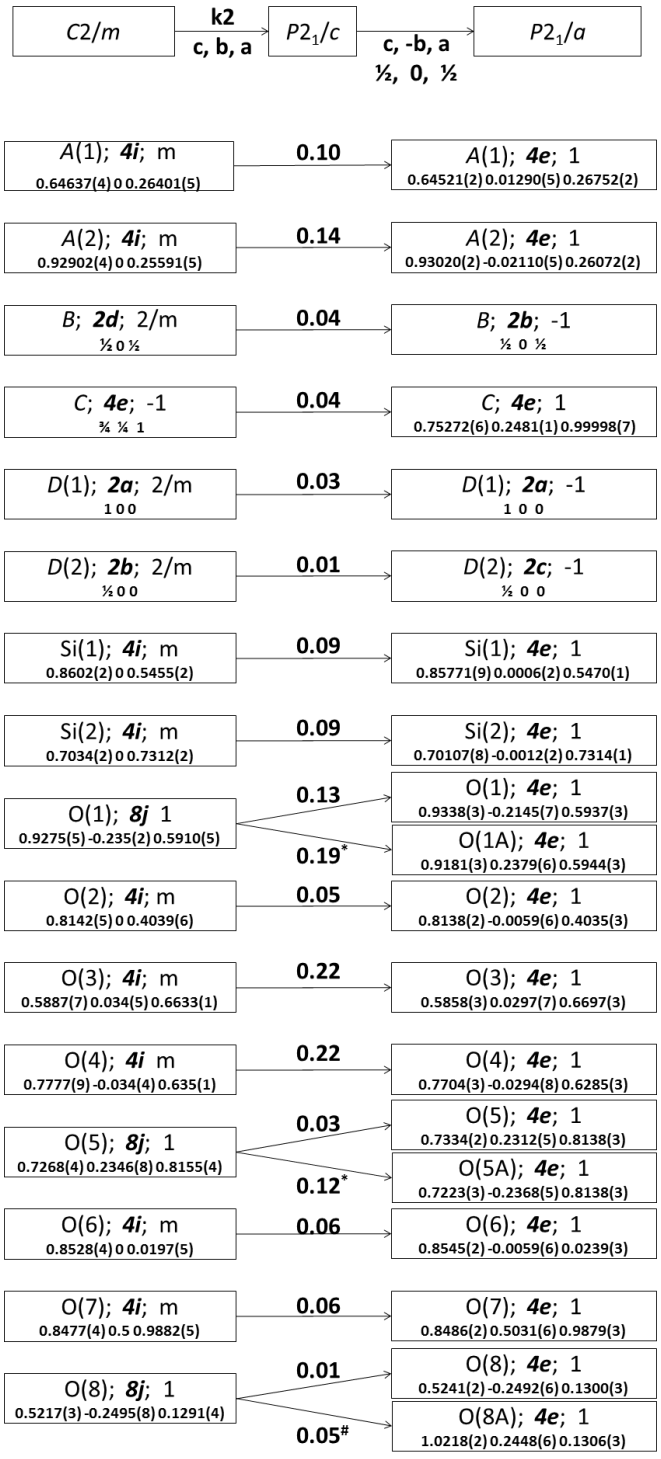

*O(1)$^{x, -y, z}$; *O(5)$^{x, -y, z}$; *O(8)$^{1/2+x, ½+y, z}$

Figure 3. The Bärnighausen (family) tree indicates a transition from aristotype *C*2/*m* to a hettotype $P2_1/a$. Above the arrows are given the shifts of atoms in Å. Below the diagram are given the three oxygen atoms that with the transformation symmetry in aristotype correspond to the O(1A), O(5A) and O(8A) atoms from the hettotype.

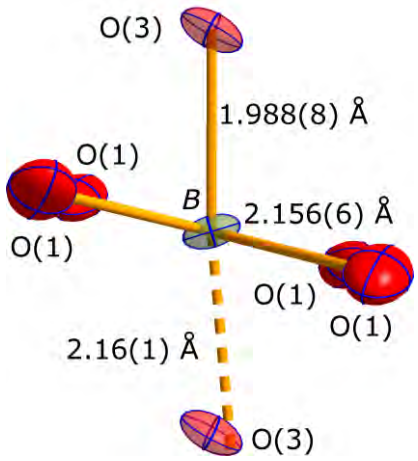

477

478 **Figure 4.** The *B*-O bonds in BO_6 coordination. The broken-off bond of 2.16 Å corresponds to the extremal

479 position of an O(3) atom.

480